Aluminum Deoxidation Equilibria in Liquid Iron: Part III—Experiments and Thermodynamic Modeling of the Fe-Mn-Al-O System

MIN-KYU PAEK, KYUNG-HYO DO, YOUN-BAE KANG, IN-HO JUNG, and JONG-JIN PAK

Deoxidation equilibria in high-Mn- and high-Al-alloyed liquid steels were studied over the entire Fe-Mn-Al composition range by both experiments and thermodynamic modeling. Effect of Mn on the Al deoxidation equilibria in liquid iron was measured by the different experimental techniques depending on the Al content. In order to confirm the reproducibility of the experimental results, the deoxidation experiments were carried out reversibly from high oxygen state by addition of Al as a deoxidizer, and from low oxygen state by addition of Fe_2O_3 or MnO as an oxygen source. For the Al-rich side, CaO flux was added on top of liquid iron in order to remove suspended Al_2O_3 inclusions in the melt. Based on the present experimental result and available critically evaluated literature data, the Al deoxidation equilibria in Fe-Mn-Al-O liquid alloy were thermodynamically modeled. The Modified Quasichemical Model was used in order to take into account a strong short-range ordering of atoms in molten state. Deoxidation equilibria and inclusion stability diagram for entire Fe-Mn-Al melt were successfully reproduced by the present model.

I. INTRODUCTION

RECENTLY, twining-induced plasticity (TWIP) steel containing a large amount of Al (0.5 to 2 mass pct) and Mn (10 to 20 mass pct) has received greater attention, because of their excellent combination of high strength and ductility over the conventional steels.[1] Although the demands for the prediction of the deoxidation limit of those steel grades have been increasing, no accurate and systematic assessments on the deoxidation behavior of high alloyed steels have been carried out up to now. As shown in Figure 1, the experimental results and thermodynamic calculations for the Al deoxidation equilibria in liquid iron do not agree among researchers, in particular at high Al concentration. This can be attributed to, first of all, the experimental difficulties at high-Al concentration region. Limit of the models[2] used is also responsible for the inconsistency. The inaccuracy would also yield a poor prediction of Al deoxidation equilibria in the multicomponent liquid such as high-Mn- and high-Al-alloyed steels. When the Al deoxidation is interpreted, the extremely strong attraction force between Al and O in liquid iron must be taken into account explicitly.[3,4]

In order to resolve the problems, the Al deoxidation equilibria in liquid iron were studied experimentally (Part I)[3] and theoretically (Part II)[4] in the previous articles of the present series. In Part I of this series,[3] the Al deoxidation equilibria in liquid iron over the entire Al concentration range of Fe-Al system were measured by the different experimental techniques depending on the Al content in the melt. The reproducibility of the deoxidation experiments was confirmed reversibly by employing the Al and Fe_2O_3 addition experiments, respectively. For the Al-rich side, the equilibrium O content was also measured by the addition of small amount of CaO flux to remove the suspended Al_2O_3 particles in the melt (For details of the experimental techniques, please see the Reference 3). The deoxidation experimental data in liquid Fe-Al[3] were thermodynamically analyzed in Part II of this series[4] using the Modified Quasichemical Model (MQM).[5,6] The strong interaction between Al and O in liquid iron was reasonably accounted for by the MQM taking into account the Short-Range Ordering (SRO) exhibited in the liquid solution. In the present study, the same experimental techniques and modeling approach were used to explain the deoxidation behavior of liquid Fe-Mn-Al over entire Al and Mn composition ranges.

There have been a few of experimental results[7–9] on the deoxidation equilibria in high-Mn- and high-Al-containing liquid steels. At low-Al concentration region ([pct Al] <0.1), Dimitrov et al.[7] reported the complex

MIN-KYU PAEK, Postdoctoral Fellow, and IN-HO JUNG, Associate Professor, are with the Department of Mining and Materials Engineering, McGill University, Montreal, QC, H3A 0C5, Canada. KYUNG-HYO DO, Graduate Student, and JONG-JIN PAK, Professor, are with the Department of Materials Engineering, Hanyang University, Ansan 426-791, Republic of Korea. Contact e-mail: jjpak@hanyang.ac.kr YOUN-BAE KANG, Associate Professor, is with the Graduate Institute of Ferrous Technology, Pohang University of Science and Technology, Pohang 790-784, Republic of Korea.

deoxidation of Mn and Al in liquid iron cosaturated with $MnAl_2O_4$ and Al_2O_3. They measured the critical Mn, Al, and O contents in Fe-Mn-Al-O melts containing Al up to 0.0026 mass pct at 1873 K (1600 °C). Ogasawara et al.[8] measured the Al and O contents in Fe-10, 30, and 50 mass pct Mn alloys in equilibrium with $MnAl_2O_4$ spinel. Using the Wagner Interaction Parameter Formalism (WIPF) with their experimental results, they determined the Gibbs free energy of formation of the spinel phase. Park et al.[9] measured the effects of Al and Mn contents on the size, composition, and three-dimensional morphologies of inclusions formed in high-Mn (10 to 20 mass pct) and high-Al (1 to 6 mass pct) alloy melts at 1873 K (1600 °C). Some of these data mentioned above were measured under the equilibrium condition.[7,8] However, their results measured at the different Al concentration ranges have not been described by a consistent thermodynamic model.

In the present study, the total Al and O contents in liquid Fe-Mn alloys in equilibrium with solid Al_2O_3 were measured at 1873 K (1600 °C) over wide composition range by the addition of Al as a deoxidizer, or addition of Fe_2O_3 or MnO as an oxygen source. In addition to this, the Al deoxidation equilibria in liquid Mn alloys were also measured at 1773 K and 1873 K (1500 °C and 1600 °C) by the addition of CaO flux for an effective removal of Al_2O_3 inclusions. Based on the critical evaluation and optimization of the present experimental results and available literature data, the Fe-Mn-Al-O liquid solution was modeled by merging the model parameters of Fe-Al-O system determined in Part II[3] and those of subsystems containing Mn. This is an extension of the present authors' previous thermodynamic modeling using the Modified Quasichemical Model for describing deoxidation equilibria in liquid steel.

II. THERMODYNAMIC MODEL USED IN THE PRESENT STUDY

The MQM in the pair approximation was used in order to take into account the SRO exhibited in the Fe-Mn-Al-O liquid solution over the entire concentration range. The detailed descriptions of the MQM and its associated notations can be found elsewhere.[4–6] The comparison of the MQM to the previous thermodynamic models such as Wagner Interaction Parameter Formalism (WIPF), Bragg–Williams Random Mixing Model (BWRMM), and the associate model has been extensively reviewed in the authors' recent studies.[4,13] Gibbs free energies of pure Fe, Mn, Al, and O were taken from Dinsdale.[14] Gibbs free energies of oxides such as solid Al_2O_3, liquid Fe_xO, solid MnO, $MnAl_2O_4$ spinel, and liquid slag of Fe-Mn-Al-O molten oxide were taken from Eriksson et al.,[15] Decterov et al.,[16] and Chatterjee and Jung,[17] respectively.

In the pair approximation of the MQM, the A and B atoms or molecules are assumed to be distributed on a quasi-lattice, and the following pair exchange reaction is considered:

$$(A\text{ - }A) + (B\text{ - }B) = 2(A\text{ - }B); \quad \Delta g_{AB} \quad [1]$$
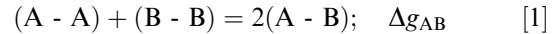
where (i-j) represents a First-Nearest Neighbor (FNN) pair. The nonconfigurational Gibbs energy change for the formation of two moles of (A-B) pairs is Δg_{AB}. Let n_A and n_B be the number of moles of A and B; n_{ij} be the number of moles of (i-j) pairs; and Z_A and Z_B be the coordination numbers of A and B. Then, the following mass balance equations for the pairs are obtained.

$$Z_A n_A = 2n_{AA} + n_{AB} \quad [2]$$

$$Z_B n_B = 2n_{BB} + n_{AB} \quad [3]$$

The pair fractions, mole fractions, and "coordination-equivalent" fractions are defined respectively as

$$X_{ij} = n_{ij}/(n_{AA} + n_{BB} + n_{AB}) \quad [4]$$

$$X_A = n_A/(n_A + n_B) = 1 - X_B \quad [5]$$

$$\begin{aligned} Y_A &= Z_A n_A/(Z_A n_A + Z_B n_B) \\ &= Z_A X_A/(Z_A X_A + Z_B X_B) = 1 - Y_B \end{aligned} \quad [6]$$

The Gibbs energy of the solution for the A-B binary solution is given by

$$G = \left(n_A g_A^\circ + n_B g_B^\circ\right) - T\Delta S^{config} + (n_{AB}/2)\Delta g_{AB} \quad [7]$$

where g_A° and g_B° are the molar Gibbs energies of pure components of A and B, and ΔS^{config} is an approximate expression for the configurational entropy of mixing given by randomly distributing the (A-A), (B-B), and (A-B) pairs in the one-dimensional Ising approximation.[5]

$$\begin{aligned} \Delta S^{config} = &-R(n_A \ln X_A + n_B \ln X_B) - R\left[n_{AA}\ln\left(\frac{X_{AA}}{Y_A^2}\right)\right. \\ &\left. + n_{BB}\ln\left(\frac{X_{BB}}{Y_B^2}\right) + n_{AB}\ln\left(\frac{X_{AB}}{2Y_A Y_B}\right)\right] \end{aligned} \quad [8]$$

Δg_{AB} is expanded in terms of the pair fractions:

$$\Delta g_{AB} = \Delta g_{AB}^\circ + \sum_{i \geq 1} g_{AB}^{i0} X_{AA}^i + \sum_{j \geq 1} g_{AB}^{0j} X_{BB}^j \quad [9]$$

where Δg_{AB}°, g_{AB}^{i0} and g_{AB}^{0j} are the parameters of the model which can be functions of temperature.

The equilibrium pair distribution is calculated by setting

$$(\partial G/\partial n_{AB})_{n_A, n_B} = 0. \quad [10]$$

This gives the equilibrium constant for the following quasichemical reaction of Eq. [1]

$$\frac{X_{AB}^2}{X_{AA}X_{BB}} = 4\exp\left(-\frac{\Delta g_{AB}}{RT}\right) \quad [11]$$

The composition of maximum SRO in each binary subsystem is determined by ratio of the coordination numbers, Z_B/Z_A, as given each of them by the following equations:

$$\frac{1}{Z_A} = \frac{1}{Z_{AA}^A}\left(\frac{2n_{AA}}{2n_{AA}+n_{AB}}\right) + \frac{1}{Z_{AB}^A}\left(\frac{n_{AB}}{2n_{AA}+n_{AB}}\right) \quad [12]$$

$$\frac{1}{Z_B} = \frac{1}{Z_{BB}^B}\left(\frac{2n_{BB}}{2n_{BB}+n_{AB}}\right) + \frac{1}{Z_{BA}^B}\left(\frac{n_{AB}}{2n_{BB}+n_{AB}}\right) \quad [13]$$

where Z_{AA}^A and Z_{AB}^A are the values of Z_A, respectively, when all nearest neighbors of an A are A's, and when all nearest neighbors of an A are B's, and where Z_{BB}^B and Z_{BA}^B are defined similarly. Z_{AB}^A and Z_{BA}^A represent the same quantity and can be used interchangeably. The coordination numbers for all pure elements (Z_{ii}^i) were selected as 6. While the coordination numbers for Fe-O (Z_{FeO}^{Fe}, Z_{FeO}^O), Al-O (Z_{AlO}^{Al}, Z_{AlO}^O), and Mn-O (Z_{MnO}^{Mn}, Z_{MnO}^O) solutions were set to 2 in order to consider the higher degree of ordering.[5] These choices were made to best represent the data, and the values of the coordination numbers selected in the present study are listed in Table I.

The Gibbs energy of the quaternary Fe-Mn-Al-O liquid solution can be expanded in a straightforward manner. Extension of the pair formation energies in each binary solution into the multicomponent system has been carried out according to Pelton and Chartrand.[6] The interpolation technique for each ternary system was determined based on the thermodynamic properties of constituent sub-binary solutions. All ternary systems containing O was treated by the "Toop-like" interpolation method where O was chosen as an asymmetric component. For the Fe-Mn-Al ternary system, Al was chosen as an asymmetric component. Thermodynamic properties of the ternary and quaternary solution estimated in this way could reproduce available experimental data as close as possible by introducing adjustable ternary parameter, $g_{AlO(Fe)}^{001}$, $g_{AlO(Mn)}^{001}$, $g_{FeAl(Mn)}^{101}$ for Fe-Al-O, Mn-Al-O, and Fe-Mn-Al systems, respectively*. All optimized model

---

*Kim and one of the present authors (YBK) recently reported a thermodynamic optimization in the Fe-Mn-Al system[18] using the same thermodynamic modeling approach where they used a revised version of Δg_{AlMn} without any ternary parameter for the liquid phase, in order to obtain good agreement with alloy phase equilibria in the Fe-Mn-Al-C system.[19] Nevertheless, the deoxidation equilibria reported in the present study were not affected by the choice of Δg_{AlMn} and the ternary parameter.

---

parameters determined in the present study are listed in Table I. All the calculations and optimizations in the present study were performed with the FactSage thermochemical software.[12]

III. EXPERIMENTAL

The Al deoxidation equilibria in Fe-Mn-Al and Mn-Al alloy melts were determined by measuring the total Al and O contents in equilibrium with pure solid Al_2O_3. Depending on the Al contents in the melts, the different experimental techniques were employed as described in Part I of the present series.[3] The deoxidation experiments were carried out using a 15-kW high-frequency induction furnace. The melt temperature was directly measured by a Pt/Pt-13 mass pct Rh thermocouple sheathed with an alumina tube (OD: 8 mm) immersed in the melt, and the temperature was accurately controlled within 2 °C by a proportional-integral-derivative (PID) controller.

A. Deoxidation by Al Addition in Fe-Mn-Al-O Melts

The Al deoxidation equilibria in liquid Fe-Mn-Al alloys were determined by adding Al into Fe-20 mass pct Mn alloy melt. 500 g of high-purity electrolytic iron and manganese contained in an Al_2O_3 crucible (OD: 56 mm, ID: 50 mm, H: 96 mm) was melted under Ar-10 pct H_2 gas for 2 hours. The initial O content in the melt prior to Al addition was 13 mass ppm. The gas was switched to dehydrated and deoxidized Ar gas, and the additions of Al (99.9 pct purity) were repeated until the Al content was up to 3.89 mass pct. After each addition, a new Al-O equilibrium was attained within 2 hours. During 20 hours duration experiment, Mn content in the melt decreased from 18.48 to 15.08 mass pct by evaporation.

B. Oxidation of Al by Fe_2O_3 and MnO Additions in Fe-Mn-Al-O Melts

In order to confirm the deoxidation experiments, the Al-O relation at high Al content was also measured in such a way that Al was oxidized and decreased by the addition of oxide as an oxygen source. 500 g of premelted Fe-22 mass pct Mn-3 mass pct Al alloy was charged and melted in a pure Al_2O_3 crucible at 1873 K (1600 °C) under Ar-10 pct H_2 gas for 2 hours. The initial O content in the melt prior to oxide addition was 3.9 mass ppm. The gas was switched to dehydrated and deoxidized Ar gas, and a predetermined amount of Fe_2O_3 or MnO powder was added onto the Fe-Mn-Al alloy melt.

C. CaO Flux Addition to Remove Al_2O_3 Particles in Mn-Al-O Melts

The ternary Mn-Al-O system is one of the important subsystems prior to the modeling of the Fe-Mn-Al-O system. Therefore, the equilibrium O content in Mn-Al melts over the entire composition range was determined in the present study. In the preliminary experiments, the reproducibility in the O analysis in the samples was poor due to the insoluble O from suspended Al_2O_3 particles in Mn-Al melts. As shown in Part I,[3] the addition of small amount of CaO was effective to remove the inclusions without disturbing the Al-O equilibrium under the saturation of Al_2O_3 in liquid iron.

Table I. Model Parameters Optimized or Used for the Fe-Mn-Al-O System in the Present Study (J/mol)

Liquid (L)—MQM (Fe, Mn, Al, O)

$Z^{Fe}_{FeFe} = Z^{Al}_{AlAl} = Z^{Mn}_{MnMn} = Z^{O}_{OO} = 6$	
$Z^{Fe}_{FeAl} = Z^{Al}_{FeAl} = Z^{Mn}_{MnAl} = Z^{Al}_{MnAl} = Z^{Fe}_{FeMn} = Z^{Mn}_{FeMn} = 6$	
$Z^{Fe}_{FeO} = Z^{O}_{FeO} = Z^{Al}_{AlO} = Z^{O}_{AlO} = Z^{Mn}_{MnO} = Z^{O}_{MnO} = 2$	
$g_{Fe},\ g_{Al},\ g_{Mn},\ g_{O}$	from[14]
Δg_{FeO}	$-142{,}867 + 8.368T$[4]
Δg_{AlO}	$-464{,}633.2 + 96.650T$[4]
Δg_{MnO}	$-192{,}464$
Δg_{FeAl}	$-20{,}292.4 + 3.347T - (1{,}673.6 + 1.255T)X_{FeFe} - 1{,}046X^{2}_{FeFe}$ $-(10{,}460 - 4.184T)X_{AlAl}$[30]
Δg_{MnAl}	$-16{,}945.2 + 3.0125T - (5857.6 - 0.418T)X_{AlAl}$ $-(1673.6 - 2.761T)X_{MnMn}$[11]
Δg_{FeMn}	$-1338.9 + 0.1674T + 418.4X_{FeFe} - 334.72X_{MnMn}$
$g^{001}_{AlO(Fe)}$	$-16{,}736$[4]
$g^{001}_{AlO(Mn)}$	$-16{,}736$
$g^{101}_{FeAl(Mn)}$	-6276

30 g of Mn-Al alloy was charged in an Al_2O_3 crucible (OD: 40 mm, ID: 30 mm, H: 50 mm) and melted using a 15 kW/50 kHz high-frequency induction furnace under an Ar-10 pct H_2 gas atmosphere at 1773 K and 1873 K (1500 °C and 1600 °C). After 2 hours of melting at desired temperatures, the gas was switched to dehydrated and deoxidized Ar gas. 2 g of CaO pellets (98 pct purity) was added onto the melt. The CaO pellets were heated at 1173 K (900 °C) for 12 hrs prior to use. After the addition of CaO pellets, a liquid slag was immediately formed on the melt surface. After 2 hours of equilibration, the top slag gradually solidified. The sample was then immediately quenched by helium gas stream and carefully sectioned for the chemical analysis.

D. Sample Analyses

The metal samples were carefully sectioned and cut for the chemical analyses. The O content in the sample was measured using the inert gas fusion-infrared absorptiometry technique (LECO, TC-600). For the analysis of Al and Mn contents, the metal samples (0.2 g) were dissolved in 20 mL HCL(1 + 1) in a glass beaker of 50 mL capacity heated in a water bath for 2 hours and analyzed by inductively coupled plasma-atomic emission spectrometry (ICP-AES, Spectro Analytical Instruments, SPECTRO ARCOS).

The oxide layer formed on the surface of Mn-Al alloy with CaO flux additions was examined by the X-ray diffraction analysis (XRD, Rigaku, D/MAX-25000/PC) to identify the phases formed after the removal of suspended Al_2O_3 particles in the melt. The inclusions formed in the liquid Mn-Al alloy were also analyzed using the potentiostatic electrolytic extraction method. For the preparation of the 10 pct AA solution, 2.5 g of tetramethyl ammonium was dissolved in 25 mL of acetyl acetone, and then 225 mL of methanol was added in a glass beaker with a capacity of 300 mL. One gram of the alloy sample was dissolved in the 10 pct AA solution under a total electric charge of 300 mA for 6 hours. The inclusions were collected by the suction filtration using a membrane filter with an open pore size of 0.1 μm. Morphology and composition of the inclusions were analyzed using scanning electron microscopy-energy dispersive X-ray spectroscopy (SEM-EDS, Hitachi, S4800).

IV. RESULTS AND DISCUSSIONS

A. Fe-Al-O System

For the prediction of deoxidation limit of high-Mn- and high-Al-alloyed steels, it is essential to have an accurate description of the Al deoxidation equilibria in liquid iron at high-Al concentration region. As shown in Figure 1, the Al deoxidation equilibria in liquid iron have been well described in the range of the normal Al-killed steels containing Al up to hundreds ppm. However, the experimental results[20–28] and calculations[20,29] at high-Al concentration region are inconsistent with each other. In order to overcome these limitations of experiments and thermodynamic analysis at high-Al concentration region, the Al deoxidation equilibria in liquid iron were measured over the entire Al concentration range (Part I)[3] and the new Al-O relation in the complete Fe-Al alloy system was successfully described using the MQM by considering the SRO exhibited in the liquid solution (Part II).[4]

In Part I of the present series,[3] it was experimentally found that the suspended alumina particles in the melt can be a main cause of the overestimation of O during the analysis. In order to minimize this effect, the initial O content in the melt was controlled as low as possible prior to Al addition by blowing Ar-H_2 gas mixture, and then the Fe-Al-O melt was equilibrated under purified Ar gas for 2 hours with the strong agitation by the high-frequency induction furnace. This helped the fast attainment of the equilibrium as well as the enough floatation time of the residual alumina particles from the melt. The present experimental results by the addition of Al were relatively lower than the calculated O content
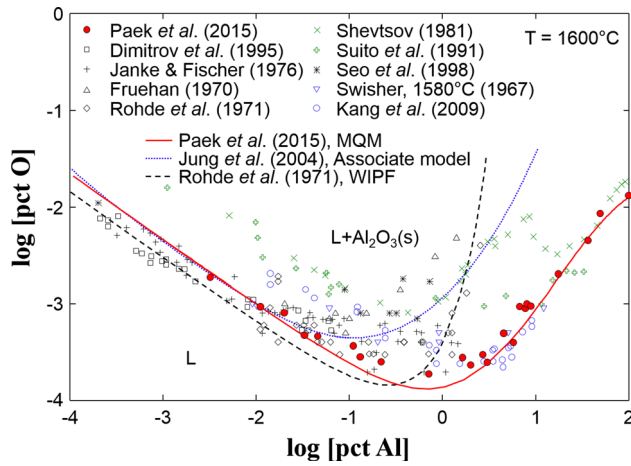
Fig. 1—Al deoxidation equilibrium in liquid iron at 1873 K (1600 °C). Lines are calculated by Rohde et al. (dashed line),[20] Jung et al. (dotted line),[29] and the present study. Symbols are experimental data.[3,20–28]

using the previous models especially at [pct Al] > 1 as shown in Figure 1. The low O level at high Al concentration in liquid iron was confirmed again by the Fe_2O_3 addition experiment that it was not a result of the oxygen deficiency.[3,27] In Al-rich side, CaO flux was added onto the Al-deoxidized melts to promote the removal of suspended Al_2O_3 particles in the melts. As shown in Figure 1, the experimental results measured in Part I are in good agreement with the lower [pct O] values of the previous data[20–28] over the whole Al composition range at 1873 K (1600 °C). These experimental techniques were also applied for the measurements of Al deoxidation equilibria in liquid Mn (Section IV–D) and Fe-Mn alloys (Section IV–E) in the present study.

The significant increase of the calculated O content by the WIPF at high Al region shown as a dashed line in Figure 1 came from neglecting the SRO between Al and O in liquid iron. Later, the strong interaction between Al and O was considered by introducing associates (Al*O and Al_2*O) in the framework of Unified Interaction Parameter Formalism (UIPF);[28] however, the experimental data measured at low Al concentration were only considered in their study. On the other hand, new Al-O relations in the complete Fe-Al alloy system measured in Part I[3] and Kang et al.'s[28] recent data at high Al concentration were adopted for the thermodynamic analysis. In order to take into account the SRO in the liquid solution, the MQM was used as discussed in Part II of the present series.[4] The new Al-O relation was reproduced well with introducing only one small ternary temperature-independent parameter because the SRO was reasonably accounted by the negative Gibbs free energy of the Eq. [1], and the nonideal mixing entropy of solution was explicitly considered in this model.[4] This emphasized the necessity of the proper consideration of the SRO for the calculation of the deoxidation equilibria in high alloyed liquid steels.
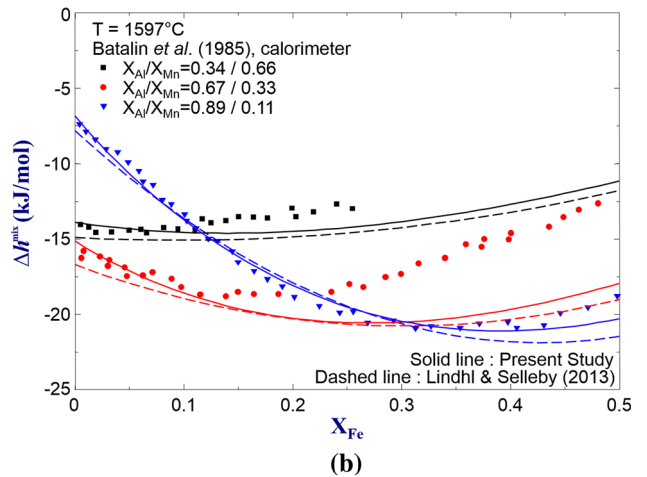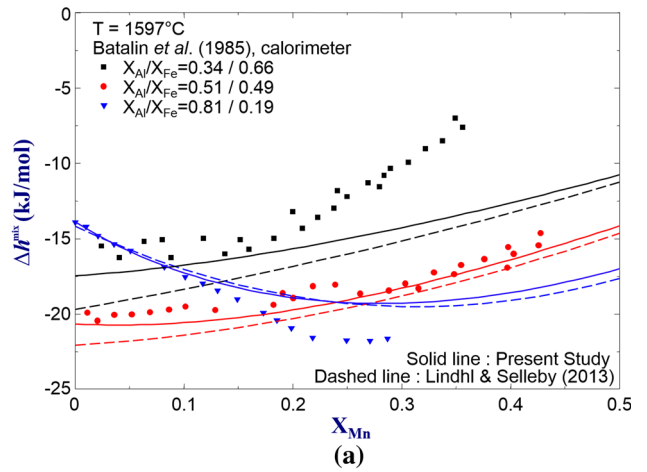

(a)

(b)

Fig. 2—Enthalpy of mixing in Fe-Mn-Al liquid alloy at (a) X_{Al}/X_{Fe} of 0.34/0.66, 0.51/0.49, and 0.81/0.19 and (b) X_{Al}/X_{Mn} of 0.34/0.66, 0.67/0.33, and 0.89/0.11 at 1597 °C.[31] (Solid lines: present study, dashed lines: Lindhl and Selleby[32]).

B. Fe-Mn-Al System

In order to calculate the deoxidation equilibria in the quaternary Fe-Mn-Al-O system, accurate liquid solution properties of the Fe-Mn-Al ternary alloy and its sub-binaries (Fe-Mn, Fe-Al, and Mn-Al systems) are required. For the optimization of the liquid solution in this ternary system, the binary MQM parameter of the Mn-Al system determined by Shukla and Pelton[11] was directly used in the present study along with those of the Fe-Al system reassessed by the authors' recent study.[30] The liquid phase in the Fe-Mn binary system optimized by Huang[10] using Bragg–Williams random mixing model was mainly adopted in the present study. Since the Fe-Mn liquid solution exhibits the ideal solution behavior, the Huang's optimization[10] was reevaluated using very small MQM parameters. By combining these binary parameters with the introduction of one small adjustable ternary parameter, the enthalpies of mixing of the Fe-Mn-Al liquid solution measured by Batalin et al.[31] at 1870 K (1597 °C) were reproduced well. Figure 2 compares the present calculation and the Lindhl and Selleby's results[32] optimized by the

Bragg–Williams random mixing model. As shown in Figures 2(a) and (b), the enthalpies of mixing of previous optimization[32] were lower than the experimental results[31] even at low Mn and low Fe region, respectively. This may be attributed to the use of the underestimated integral enthalpy of mixing in Fe-Al and Mn-Al binary systems.[33,34] On the other hand, the present calculation of the enthalpies of mixing in the Fe-Mn-Al system shown as solid lines in Figure 2 agrees very well with Batalin et al.'s[31] results from binary data on the y-axis to the high alloyed ternary liquid solution.

C. Fe-Mn-O System

There have been some experimental data of the O solubility in pure Mn melt in equilibrium with solid MnO. However, the reported O solubility data are scattered significantly as shown in Figure 3. Shenck et al.[35] measured the O solubility using an induction furnace under deoxidized Ar atmosphere. However, there were noticeable discrepancies because of the impurities in their samples (N: 127-620 ppm, Fe: 1100-2900 ppm, C: 190-742 ppm, and Si: ~100ppm). Chen[36] measured the O solubility in the samples taken from Mn/MnO interface due to the experimental difficulties by the low O potential and high vapor pressure of Mn. Grundy et al.[37] adopted the O solubility in liquid Mn reported by Jacob[37] for their optimization of the Mn-O system. However, Jacob's data[38] were indirectly obtained by evaluating the equilibrium relations among MnO, Al_2O_3, and $MnAl_{2+2x}O_{4+3x}$. Wang and Sundman[39] optimized this binary system by adopting the data evaluated by Jacob[38] and the experimental results measured by Simenov et al.[40] in spite of huge difference between them. For these reasons, in the present study, the liquid solution property of the binary system was determined by the correlation with the experimental results in the Fe-Mn-O ternary system. The Gibbs free energy of the Mn-O pair exchange reaction, Δg°_{MnO} was determined to reproduce the Mn-O relation of the Mn-rich side in the Fe-Mn melt at 1873 K (1600 °C) measured by Shevtsov et al.[41] and its temperature dependence of the relation measured by Takahashi and Hino,[42] respectively. As a result, the calculated O solubility in pure Mn melt fitted reasonably well with Schenck et al.'s[35] data as shown by a solid line in Figure 3.

Although the Mn deoxidation in liquid iron has been studied by many researchers, most of them were discussed in limited Mn concentration ranges.[7,41–47] On the other hand, in the present study, the deoxidation equilibria in the Fe-Mn-O system were interpreted over the whole composition range from the solid solution of Fe_xO-MnO to liquid slag saturation as shown in Figure 4. Using the binary model parameters of the Fe-O system determined in Part II,[4] and those of the Fe-Mn and Mn-O systems determined in the present study, no ternary parameter was required to reproduce the reported experimental data measured at various composition and temperature ranges. The peaks marked on the curves give the composition corresponding to the
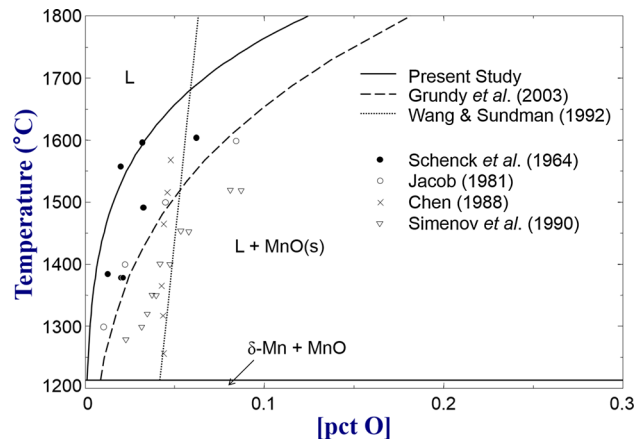

Fig. 3—O solubility in liquid Mn in equilibrium with solid MnO. Lines are calculated by Grundy et al. (dashed line),[37] and Wang and Sundman (dotted line),[39] and the present study. Symbols are experimental data.[35,36,38,40]
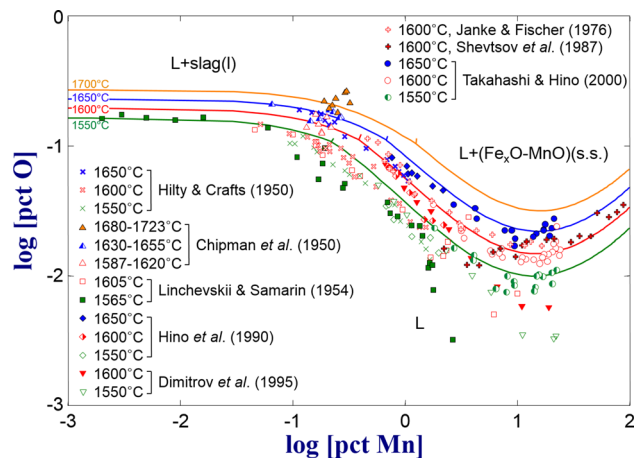

Fig. 4—Comparison between experiments[7,41–47] and model calculations for Mn-O relation in liquid iron at various temperatures from 1823 K to 1973 K (1550 °C to 1700 °C).

three-phase univariant at which the melt is co-saturated with liquid slag and Fe_xO-MnO solid solution. The present optimization in the low-Mn content region saturated with liquid slag agreed very well with Chipman et al.[44] and Linchevskii and Samarin's[45] data. At the higher-Mn content region saturated with Fe_xO-MnO solid solution, the Mn deoxidation equilibria at 1873 K (1600 °C) measured over a wide composition range by Janke and Fischer[46] and Shevtsov et al.[41] and the temperature effect of the relation measured by Takahashi and Hino[42] were reproduced well. Figure 5 shows the optimized O partial pressure in a form of logarithm as a function of the Mn content in the Fe-Mn-O system. Linchevskii and Samarin[45] measured the Mn and O contents under controlled atmosphere by H_2O and H_2 gas mixture. Janke and Fischer[46] and Dimitrov et al.[7] measured the activity of O by the Electromotive Force (EMF). As shown in the figure, the present optimization agreed very well with the evaluated P_{O_2} from their H_2/H_2O partial pressures[45] and a_O[7,46] data.

D. Mn-Al-O System

No available experimental result and thermodynamic description have been reported in this system. In the present authors' preliminary experiments, it was found that the reproducibility in the O analysis was very poor at such high-Al content region due to the suspended Al_2O_3 particles in liquid Mn-Al alloy. Therefore, in the present study, the Al deoxidation equilibria in pure Mn melts were measured at 1773 K and 1873 K (1500 °C and 1600 °C) with CaO flux addition to promote the removal of suspended Al_2O_3 particles in the melt. The experimental results are summarized in Table II, and some of the data will be used to verify the Al deoxidation equilibria in Fe-Mn-Al-O melt at Al-rich side in the subsequent section.

Figure 6 shows the XRD pattern of the slag sample taken from the interface between the Mn-Al alloy and the oxide layer formed by the CaO addition. The $CaO \cdot Al_2O_3$ and $2CaO \cdot MnO_2$ phases were formed by absorbing Al_2O_3 and MnO particles suspended in the melt, but at the same time, the slag held pure Al_2O_3 particles at the interface as shown by the XRD analysis.

Figure 7 shows the SEM morphology and EDS analysis of the oxide inclusion extracted from Mn-Al alloy melt. All inclusions were identified as pure Al_2O_3. In addition, there was no phase formed at the interface between metal and Al_2O_3 crucible after CaO addition. Therefore, it can be concluded that the addition of CaO flux was effective to remove suspended Al_2O_3 particles and it did not affect the Al-O relation in the melt in equilibrium with pure solid Al_2O_3 ($a_{Al_2O_3} = 1$) under the present experimental condition.

The present results along with the O solubility in pure Al melt determined in Part I[3] were used for the optimization of the liquid solution in the Mn-Al-O system over the whole composition range as shown in Figure 8. One ternary parameter, $g_{AlO(Mn)}^{001}$ was introduced in order to describe the present experimental results more accurately. Indeed, the $g_{AlO(Mn)}^{001}$ value is equal to the ternary parameter in Fe-Al-O system, $g_{AlO(Fe)}^{001}$ determined in Part II.[4] It should be noted that the effects of Fe on the Al-O pairs and that of Mn are very similar. This can be attributed to the Fe-Mn system exhibiting an ideal solution behavior.
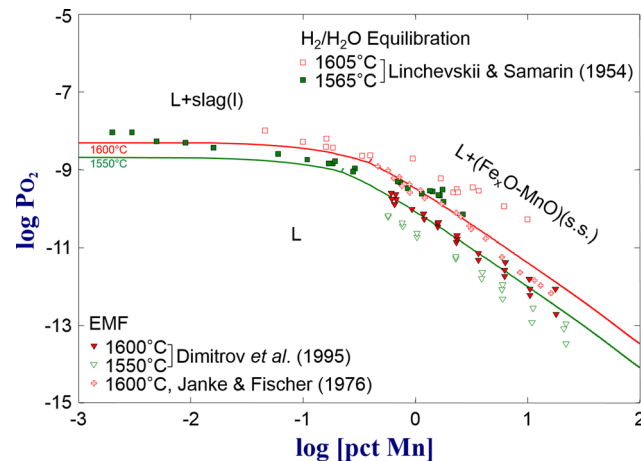

Fig. 5—Calculated O partial pressure in Fe-Mn-O melts along with experimental data.[7,45,46]
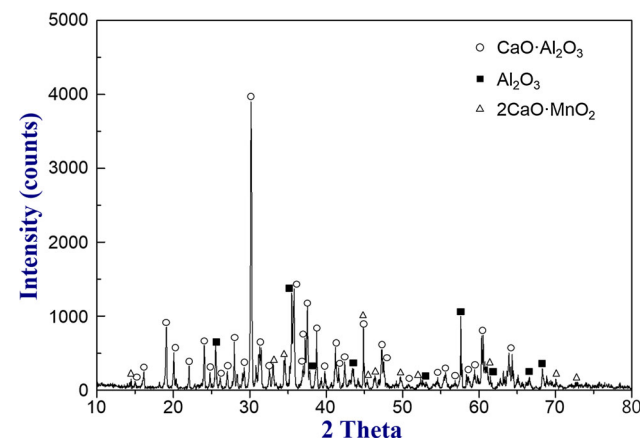
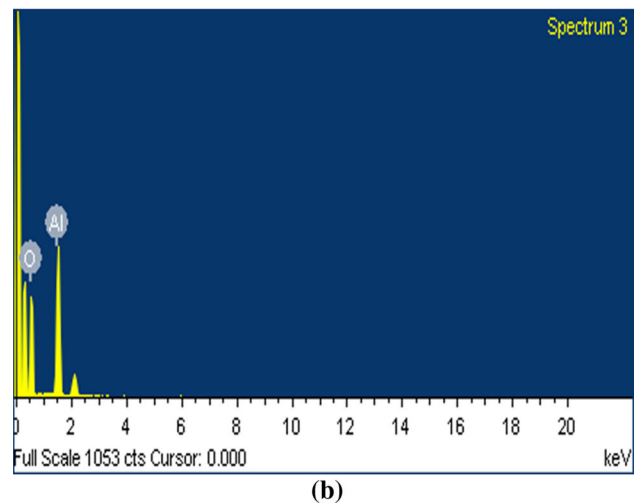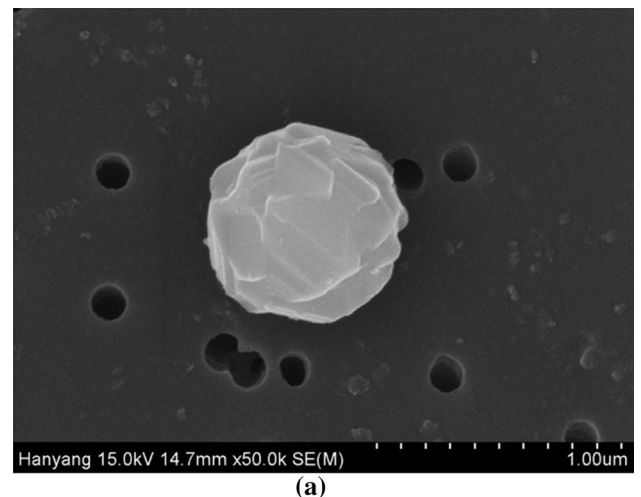Fig. 6—XRD data of oxides formed on the surface of Mn-14.12 mass pct Al alloy melt.

(a)

(b)

Fig. 7—(a) SEM image and (b) EDS spectrum of inclusion in Mn-14.12 mass pct Al alloy melt.

E. Fe-Mn-Al-O System

In order to establish the effect of Mn on the Al deoxidation equilibria in liquid iron over the wide composition range, the Al deoxidation equilibria in Fe-Mn-Al-O melts in equilibrium with pure solid Al_2O_3 were reversibly measured at 1873 K (1600 °C) by the addition of Al as a deoxidizer and the oxide (Fe_2O_3 or MnO) as an oxygen source as shown in Figure 9. The experimental results are also summarized in Table II. In the region of the [pct Al] up to 3.89 mass pct, pure Al was added in Fe-Mn-O alloy melt. The O content decreased by the addition of pure Al and then increased again after a minimum point showing the similar behavior as the Fe-Al-O system in Part I.[3] The reproducibility of the Al addition experiment was confirmed by the addition of Fe_2O_3 or MnO into Fe-22 mass pct Mn-3 mass pct Al melt. The Al and O contents simultaneously decreased along the Al deoxidation experiments by the addition of the oxides.

Figure 9 compares the present experimental results and the prediction of the [pct Al]-[pct O] relation in
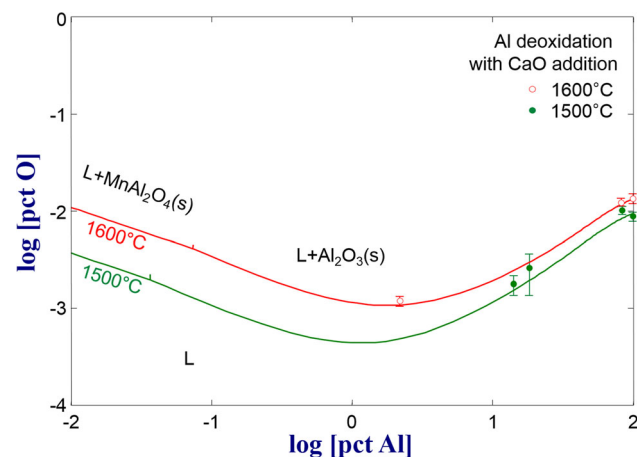

Fig. 8—Calculated [pct Al]-[pct O] relation in liquid Mn with the present experimental results.
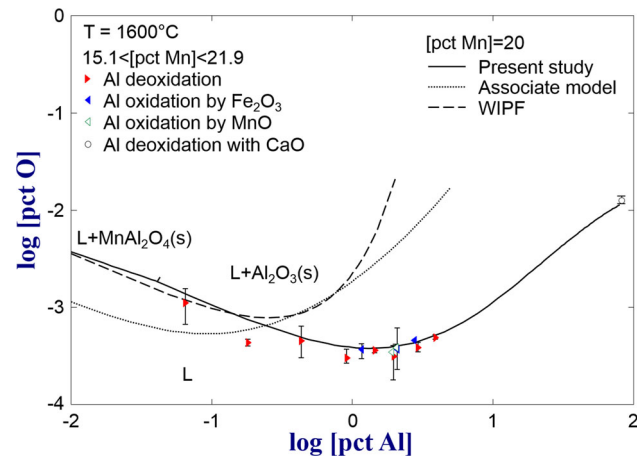

Fig. 9—Al deoxidation equilibria in Fe-Mn-Al-O melt at 1873 K (1600 °C). Lines are calculated by the WIPF (dotted line),[48] the associate model (dashed line),[29] and the present study.

Fe-20 mass pct Mn-Al alloy melt at 1873 K (1600 °C) according to the thermodynamic models such as the MQM, WIPF, and associate model. The equilibrium O content in Mn-82.2 mass pct Al alloy melt measured by the addition of CaO flux (D-2 in Table II) was also plotted together for the verification of the deoxidation equilibria in Fe-Mn-Al-O melt at the Al-rich side. The present experimental results measured by various techniques are shown to be consistent with each other. The Al deoxidation equilibria in Fe-Mn-Al-O melt were reproduced very well using the MQM without any additional parameter for this quaternary system. The dotted line is the calculated deoxidation equilibria using WIPF with the recommended parameters by the Japan Society for the Promotion of Science (JSPS),[48] and the dashed line is the calculated result by Unified Interaction Parameter Formalism (UIPF) with three associates (Al*O, Al_2*O, and Mn*O).[29] As was discussed in Part II of the present series,[4] the interaction parameter formalism cannot be extended into high-concentration region. Therefore, the present thermodynamic modeling is superior to the previous modeling approaches.

In contrast to the previous models, the MQM shows the wide applicability to describe the liquid solution properties over the complete concentration range. As shown in Figure 10, the Al deoxidation equilibria in Fe-Mn-Al-O melts can be predicted over the entire Mn concentration range from pure Fe to pure Mn melt by the one set of thermodynamically consistent equation of the MQM with the identical model parameters. At high-Al concentration region, the present experimental results and predictions are in good agreement with Park et al.'s[9] results measured at 10 and 20 mass pct Mn. While Ogasawara et al.'s[8] data at low-Al concentration region are lower than the present model predictions, in general, Mn increases the equilibrium O content at the same Al concentration, because of stronger attraction force between Mn and O than that between Fe and O. However, it was not easy to find the tendency of the Mn effect from their results.[8] As shown in the figure, the O content at the same Al concentration was not proportionally increased with the Mn concentration in the melts. In particular, the effect of Mn on the Al deoxidation in Fe-Mn-Al-O melts can be almost negligible at the Al-rich side. This may be explained by the variation of pair fractions in the melt. Figure 11 shows the equilibrium fractions of various pairs in Fe-20 mass pct Mn-Al-O melt calculated by the MQM. The equilibrium O content obtained in the present model calculation is a result of sum of O in various FNN pairs containing O ((Fe-O), (Mn-O), (Al-O), and (O-O)). As can be seen in Figure 11(a), the (Al-Al) pairs become dominant with increasing Al content, and the (Fe-O) and (Mn-O) pairs were consumed to form (Al-O) and (O-O) pairs as shown in Figure 11(b). This means that there are a few chances to form (Fe-O) and (Mn-O) pairs at high-Al concentration region ([pct Al] > ~10). Therefore, the deoxidation curves at Al-rich side were convergent in the Fe-Mn-Al-O system as shown in Figure 10.

Figure 12 shows a predicted inclusion stability diagram for the Fe-Mn-Al-O system using the present

| Temp. [K (°C)]	Exp. No	Method	[pct Mn]	[pct Al]	[pct O]
1873 (1600)	A1	Al addition	18.48	0.0647	0.00111
	A2		17.75	0.1812	0.00043
	A3		17.41	0.4303	0.00044
	A4		17.19	0.9081	0.00030
	A5		16.83	1.450	0.00036
	A6		16.33	1.968	0.00031
	A7		15.91	2.932	0.00038
	A8		15.08	3.892	0.00048
	B1	Fe$_2$O$_3$ addition	21.86	2.761	0.00045
	B2		18.28	2.092	0.00036
	B3		18.68	1.171	0.00037
	C1	MnO addition	21.07	2.057	0.00038
	C2		20.70	1.918	0.00034
	D1	CaO addition	97.80	2.191	0.00118
	D2		17.82	82.16	0.01200
1773 (1500)	D3	CaO addition	85.87	14.12	0.00176
	D4		81.74	18.25	0.00257
	D5		16.59	83.40	0.01010
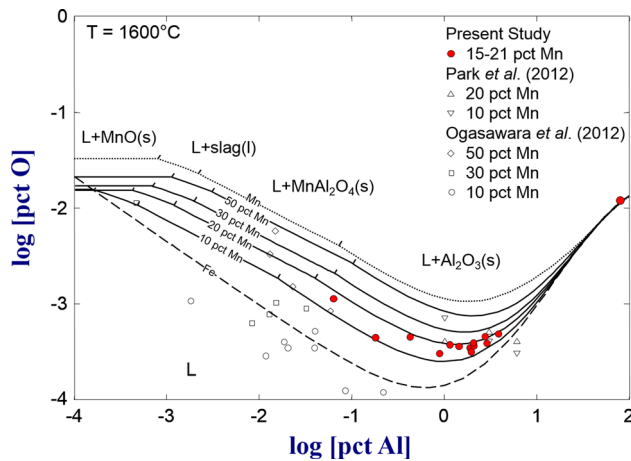
Fig. 10—Calculated Al deoxidation equilibria in Fe-Mn-Al alloy melts at 1873 K (1600 °C) with experimental data.[8,9]

thermodynamic modeling. The present experimental results and literature data are also shown by symbols.[7–9] As shown in the figure, most region of the stability diagram is occupied by Al$_2$O$_3$. This means that most inclusions formed as deoxidation product in high-Mn- and high-Al-alloyed steels would be alumina unless the Mn content is very high. Typical Al content in normal C steel is a few hundreds ppm and it is much higher in TWIP steel, and the equilibrium phase of oxide inclusions in those steels should be alumina. This is in agreement with the report of Park et al.[9] who found majority of oxide inclusions in Fe-(10 to 20 mass pct) Mn-(1 to 6 mass pct) Al-containing steel were alumina. This figure may be used as a useful tool for quick check of possible inclusion phases in high-Mn and high-Al steels.

For the validity check of this figure, some available experimental data were mentioned here. The O contents in steels in equilibrium with Al$_2$O$_3$ and MnAl$_2$O$_4$ were
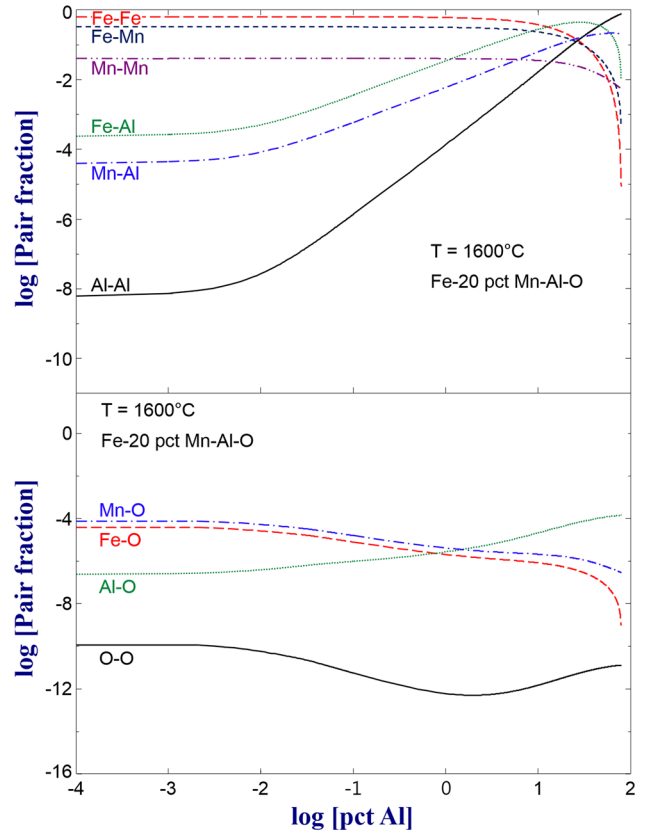

Fig. 11—Predicted pair fractions of various pairs in Fe-20 mass pct Mn-Al-O melt at 1873 K (1600 °C).

measured by Dimitrov et al.[7] The O content is lower than that predicted in the present study. Moreover, the critical Mn and Al contents in Fe-Mn-Al-O melts cosaturated with MnAl$_2$O$_4$ and Al$_2$O$_3$ are inconsistent with the calculated boundary of the oxides. It may be caused by the experimental and analytical difficulties to
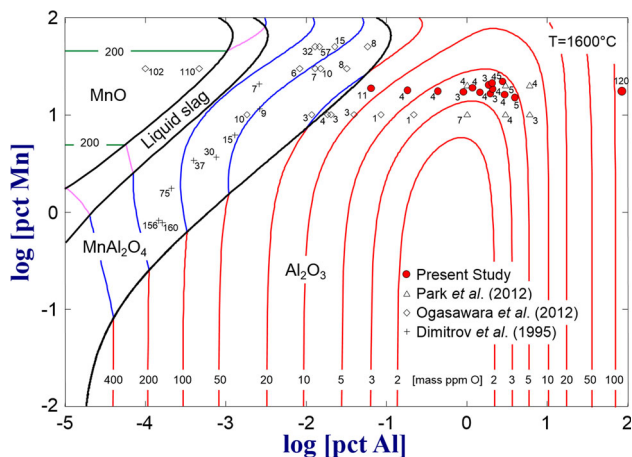
Fig. 12—Predicted inclusion stability diagram for the Fe-Mn-Al-O system with experimental results.[7–9]

obtain an accurate cosaturated value at such low-Al concentration. As mentioned earlier, the O content measured by Ogasawara et al.[8] was also lower than the present calculation. Even though they reported that all their samples were equilibrated with the $MnAl_2O_4$ spinel phase, most of their results at 10 mass pct Mn fall in the Al_2O_3 stable region. In order to interpret their result, Gibbs free energy of formation of $MnAl_2O_4$ spinel phase should be ~−130 kJ/mol at 1873 K (1600 °C).[8] This is an unacceptably high value compared to the well-known value of −28 ± 4 kJ/mol at 1573 K to 1973 K (1300 °C to 1700 °C).[7,49–53] On the other hand, the O content reported by Park et al.[9] is in good agreement with the present model calculation. Therefore, the present inclusion stability diagram can be considered to be most reasonable and updated. This type of diagram can be predicted for different temperatures in order to track phase change of inclusions during steelmaking and casting process.

V. CONCLUSION

The deoxidation equilibria in high-Mn- and high-Al-alloyed liquid steel were experimentally determined over the entire composition range of Fe-Al-Mn system. By considering the Short-Range Ordering exhibited in the liquid solution, the Al deoxidation equilibria and the inclusion stability diagram for Fe-Mn-Al-O melts were reproduced very well using the binary model parameters with only three ternary temperature-independent parameters. These are demonstrated with the applicability of the MQM for the liquid solution exhibiting strong interaction and its expandability to the multicomponent system for the description of the complex deoxidation equilibria in the high alloyed liquid steels. According to the present experimental and thermodynamic modeling results, the deoxidation product for the steel containing more than 0.1 mass pct Al is always Al_2O_3 regardless of Mn concentration, and

therefore the equilibrium oxygen concentration is mostly controlled by Al in liquid Fe-Mn-Al steel.

REFERENCES

1. O.J. Kwon: *Proceedings of 1st International Conference on High Manganese Steels*, Yonsei University, Seoul, Korea, 2011, p. 40.
2. C. Wagner: *Thermodynamics of Alloys*, Addision-Wesley Press, Cambridge, MA, 1952, pp. 47–51.
3. M.K. Paek, J.M. Jang, Y.-B. Kang, and J.J. Pak: *Metall. Mater. Trans. B*, 2015, vol. 46B, pp. 1826–36.
4. M.K. Paek, J.J. Pak, and Y.-B. Kang: *Metall. Mater. Trans. B*, 2015, vol. 46B, pp. 2224–33.
5. A.D. Pelton, S.A. Degterov, G. Eriksson, C. Robelin, and Y. Dessureault: *Metall. Mater. Trans. B*, 2000, vol. 31B, pp. 651–9.
6. A.D. Pelton and P. Chartrand: *Metall. Mater. Trans. A*, 2001, vol. 32A, pp. 1355–60.
7. S. Dimitrov, A. Weyl, and D. Janke: *Steel Res.*, 1995, vol. 66, pp. 87–92.
8. Y. Ogasawara, T. Miki, and T. Nagasaka: *CAMP-ISIJ*, 2012, vol. 25, p. 240.
9. J.H. Park, D.J. Kim, and D.J. Min: *Metall. Mater. Trans. A*, 2012, vol. 43A, pp. 2316–24.
10. W. Huang: *Calphad*, 1989, vol. 13, pp. 243–52.
11. A. Shukla and A.D. Pelton: *J. Phase Equilib. Diff.*, 2009, vol. 30, pp. 28–39.
12. C.W. Bale, E. Bélisle, P. Chartrand, S.A. Decterov, G. Eriksson, K. Hack, I.H. Jung, Y.-B. Kang, J. Melançon, A.D. Pelton, C. Robelin, and S. Petersen: *Calphad*, 2009, vol. 33, pp. 295–311.
13. M.K. Paek, S. Chatterjee, J.J. Pak, and I.H. Jung: *Metall. Mater. Trans. B*, 2016, vol. 47B, pp. 1243–62.
14. A.T. Dinsdale: *Calphad*, 1991, vol. 15, pp. 317–425.
15. G. Eriksson and A.D. Pelton: *Metall. Mater. Trans. B*, 1993, vol. 24B, pp. 807–16.
16. S.A. Decterov, E. Jak, P.C. Hayes, and A.D. Pelton: *Metall. Mater. Trans. B*, 2001, vol. 32B, pp. 643–57.
17. S. Chatterjee and I.H. Jung: *J. Eur. Ceram. Soc.*, 2014, vol. 34, pp. 1611–21.
18. M.-S. Kim and Y.-B. Kang: *J. Phase Equilib. Diffus.*, 2015, vol. 36, pp. 453–70.
19. M.-S. Kim and Y.-B. Kang: *Calphad*, 2015, vol. 51, pp. 89–103.
20. L.E. Rohde, A. Choudhury, and M. Wahlster: *Arch. Eisenhüttenwes.*, 1971, vol. 42, pp. 165–74.
21. J.H. Swisher: *Trans. Metall. Soc. AIME*, 1967, vol. 239, pp. 123–124.
22. R.J. Fruehan: *Metall. Trans.*, 1970, vol. 1, pp. 3403–10.
23. D. Janke and W.A. Fischer: *Arch. Eisenhüttenwes.*, 1976, vol. 47, pp. 195–8.
24. V.E. Shevtsov: *Russ. Metall.*, 1981, vol. 1, pp. 52–7.
25. H. Suito, H. Inoue, and R. Inoue: *ISIJ Int.*, 1991, vol. 31, pp. 1381–8.
26. S. Dimitrov, A. Weyl, and D. Janke: *Steel Res.*, 1995, vol. 66, pp. 3–7.
27. J.D. Seo, S.H. Kim, and K.R. Lee: *Steel Res.*, 1998, vol. 69, pp. 49–53.
28. Y.J. Kang, M. Thunman, D. Sichen, T. Morohoshi, K. Mizukami, and K. Morita: *ISIJ Int.*, 2009, vol. 49, pp. 1483–9.
29. I.H. Jung, S.A. Decterov, and A.D. Pelton: *Metall. Mater. Trans. B*, 2004, vol. 35B, pp. 493–507.
30. A.T. Phan, M.K. Paek, and Y.B. Kang: *Acta Mater.*, 2014, vol. 79, pp. 1–15.

31. G.I. Batalin, T.P. Bondarenko, and V.S. Sunavtsova: *Dopov. Nat. Akad. Nauk. Ukr.*, 1985, vol. 4, pp. 76–78.
32. B.B. Lindahl and M. Selleby: *Calphad*, 2013, vol. 43, pp. 86–93.
33. B. Sundman, I. Ohnuma, N. Dupin, U.R. Kattner, and S.G. Fries: *Acta Mater.*, 2009, vol. 57, pp. 2896–908.
34. Y. Du, J. Wang, J. Zhao, J.C. Schuster, F. Weitzer, R. Schimid-Fetzer, M. Ohno, H. Xu, Z.K. Liu, S. Shang, and W. Zhang: *Int. J. Mater. Res.*, 2007, vol. 98, pp. 855–71.
35. H. Schenck, M.G. Frohberg, and R. Nünninghoff: *Arch. Eisenhüttenwes.*, 1964, vol. 35, pp. 269–77.
36. Q. Chen: *Acta Metall. Sinica*, 1988, vol. 24, pp. 440–41.
37. A.N. Grundy, B. Hallstedt, and L.J. Gauchler: *J. Phase Equilib.*, 2003, vol. 24, pp. 21–39.
38. K.T. Jacob: *Metall. Mater. Trans. B*, 1981, vol. 12B, pp. 675–78.
39. M. Wang and B. Sundman: *Metall. Mater. Trans. B*, 1992, vol. 23B, pp. 821–31.
40. S. Simenov, L. Ivanchev, and D. Popivanov: *Izv. Vyssh. Uchebn. Zaved. Chern. Metall.*, 1990, vol. 11, pp. 20–2.
41. V.E. Shevtsov, E.E. Merker, and V.P. Luzgin: *Izy. Vuzov. Cher. Met.*, 1987, vol. 9, pp. 4–6.
42. K. Takahashi and M. Hino: *High Temp. Mat. Proc.*, 2000, vol. 19, pp. 1–10.
43. D.C. Hilty and W. Crafts: *J. Met. Trans. AIME*, 1950, vol. 188, pp. 425–36.
44. J. Chipman, J.B. Gero, and T.B. Winkler: *Trans. AIME*, 1950, vol. 188, pp. 341–45.
45. B.V. Linchevskii and A.M. Samarin: *Izv. AN SSS. Otd. Tekh. Nauk.*, 1957, vol. 2, pp. 9–18.
46. D. Janke and W.A. Fischer: *Arch. Eisenhüttenwes.*, 1976, vol. 47, pp. 147–51.
47. M. Hino, I. Kikuchi, A. Fujisawa, and S. Banya: *Proceedings of 6th International Iron Steel Congress*, Nagoya, Japan, 1990, vol. 1, pp. 264–71.
48. The 19th Committee in Steelmaking: *Thermodynamic Data for Steelmaking*, The Japan Society for Promotion of Science, Tohoku University Press, Sendai, Japan, 2010, pp. 10–13.
49. K.T. Jacob: *Can. Metall. Q.*, 1981, vol. 20, pp. 89–92.
50. Y. Zhao, K. Morita, and N. Sano: *Metall. Mater. Trans. B*, 1995, vol. 26B, pp. 1013–17.
51. L.M. Lenev and I.A. Novokahtskii: *Izv. Akad. Nauk. SSSR Metally*, 1966, vol. 3, pp. 73–78.
52. C.K. Kim and A. McLean: *Metall. Mater. Trans. B*, 1979, vol. 10B, pp. 575–84.
53. M. Timucin and A. Muan: *J. Am. Ceram. Soc.*, 1992, vol. 75, pp. 1399–406.